

Optimal fractal dimension on grain structure robot laser-hardened tool steel

Babic, M.^{a,*}, Balic, J.^b, Kokol, P.^c

^aEMO-Orodjarna d.o.o., Celje, Slovenia

^bFaculty of Mechanical Engineering, University of Maribor, Slovenia

^cFaculty of Electrical Engineering and Computer Science, University of Maribor, Slovenia

ABSTRACT

In order to optimize the structure and properties of tool steel, it is necessary to take into account the effect of the self-organization of a dissipative structure with fractal properties at load. Fractal material science researches the relationship between the parameters of fractal structures and the dissipative properties of tool steel. This paper describes the application of fractal dimension in robot laser-hardening specimens. By using fractal dimensions, changes in the structure can be determined because the fractal dimension is a present indicator of the complexities of the sample forms. We hardened tool steel at different speeds and different temperatures. By researching the fractal dimensions of the microstructures of the hardened specimens we could better understand the effects of the parameters of robot cells on the material. We show the experimental results and an analysis of those fractal patterns that occur during robot laser hardening with the different parameters of temperature and speed. Finally, we present the relationship between the fractal dimensions and the parameters of temperature and speed of robot laser hardening. The hardening of various metal alloys showed that when melting occurs, fractal geometry can be used to calculate the fractal dimension. The dependence of the fractal dimension on the hardness was ascertained. This finding is important when we realize that certain alloys mix poorly because they have different melting temperatures but such alloys have a much higher hardness and better technical characteristics.

© 2014 PEI, University of Maribor. All rights reserved.

ARTICLE INFO

Keywords:

Fractal dimension
Robot
Laser
Hardening

*Corresponding author:

babicster@gmail.com
(Babic, M.)

Article history:

Received 31 October 2013
Revised 13 May 2014
Accepted 7 July 2014

1. Introduction

Of all microscopic methods, electron microscopy images give the best resolution, the most accurate information of the distribution of crystals in a building, the best morphology of the various structural types, and the best structural surface topography. Fractal geometry provides a new approach in describing the structure of various illegal structures. Fractal theory has also been used in the field of materials science. Models of fractal lines and surfaces were created to describe the properties of the microstructure of materials [1]. The subject of fractals can be used to assist in the analysis of surfaces encountered in robot laser hardening. It should be noted that the morphology of a surface will change if material is hardened with robot laser cells. Analysis of fractal dimensions is a method used to study the surface properties of materials. Fractal dimension [2] is a property of fractals that is maintained over all magnifications and is therefore well defined, but in addition, it also reveals the complexity of the fractal. In general, we cannot calculate the fractal dimension for the above-mentioned procedure, as this is possible only on pure

mathematical constructs, and not by nature. In practical terms, to determine the dimensions the most used method is that “of counting boxes” (box-counting dimension), which studies fractal cover using a square grid, which is then reduced and the change in the number of squares needed to cover the entire crowd observed. We face many problems in robot laser hardening [3]. Robot laser hardening [4] with an overlapping laser beam is particularly interesting. The result is, of course, an approximation, which is calculated by the desired number of places.

In this paper, fractal analysis is used to determine how parameters of robot laser hardening affect the hardness of the hardened material. Robot laser surface hardening heat treatment [5-6] is complementary to conventional flame or inductive hardening. The energy source for laser hardening is the laser beam, which heats up very quickly, and works on the metal surface area of points up to 1.5 mm and a hardness of 65 HRC. Laser hardening is a process of projecting features, such as non-controlled energy intake, high-performance constancy and an accurate positioning process. A hard martensitic microstructure provides improved surface properties, such as wear resistance and high strength [7-8]. Fractal analysis [9-10] is useful when classical geometry cannot be sufficiently useful to precisely describe the results of irregular facilities. A profound feature of fractals is the fractal dimension D [11-13], which provides an important view of the physical properties of various materials.

This article describes the fractal structure [14] of robot laser-hardened tool steel. Fractal patterns have been found in different mechanical properties of hardened materials (Mandelbrot 1982, Feder 1988). Fractal features have also been observed in mechanical computer simulations, which can be explained by Gauss-Marc fractal random fields. In this work, we have used a scanning electronic microscope (SEM) [15-16] to research for and analyse the fractal structure of robotic laser-hardened material. The aim of the research is to ascertain how robotic laser cell parameters for optimal tempering affect the fractal dimension of hardened material.

2. Experimental method and materials preparation

The study was undertaken using tool steel standard label DIN standard 1.7225. The chemical composition of the material was 0.38-0.45 % C, maximum of 0.4 % Si, 0.6-0.9 % Mn, maximum of 0.025 % P, maximum of 0.035 % S, and 0.15-0.3 % Mo. The specimen test section was in a cylindrical form with dimensions of 25×10 mm. After hardening, the test specimen was cut into smaller parts. Tool steel was forged with a laser at different speeds and at different powers. So we changed the two parameters: speed v was set to 2-5 mm/s in steps of 1 mm/s, and temperature T to 1000-1400 °C in steps of 50 °C. During all these tests, we recorded the microstructure.

We recorded the hardened surface area as well as the deep hardened zone of the clips. Of interest to us was whether the robotic laser hardening parameters for different fractal structures found microparticles. Also, we wanted to know or ascertain the fractal structure of the optimal parameters of hardening. Fig. 1 shows the longitudinal and transverse cross section of hardened tool steel. In Figs. 2, 3, 4, and 5 the microstructures of tempered tool steel at different magnifications are shown.



Fig. 1 Hardened tool steel

Prior to testing, the specimens were subjected first to mechanical and then to electrolytic polishing [17] in $\text{H}_3\text{PO}_4 + \text{CrO}_3$ at the IMT Institute of Metals and Technology, Ljubljana, Slovenia. After polishing we made images with a microscope. First, we made recordings using an optical microscope and then with an electron microscope. Images were made using a JEOL JSM-7600F field emission scanning electron microscope. Irregular surface textures with a few breaks, represented by black islands, were revealed (Fig. 2).

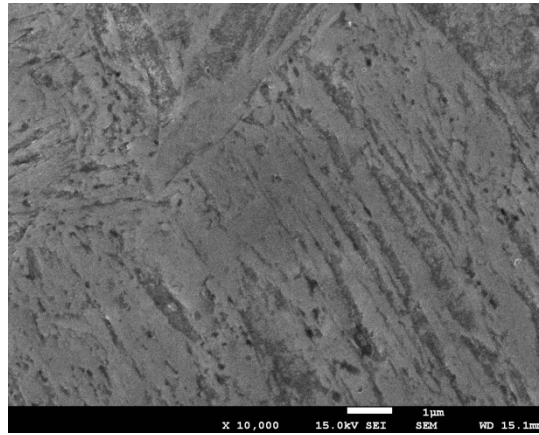


Fig. 2 SEM image of 1000 °C and 2 mm/s at 50000× magnification on the surface

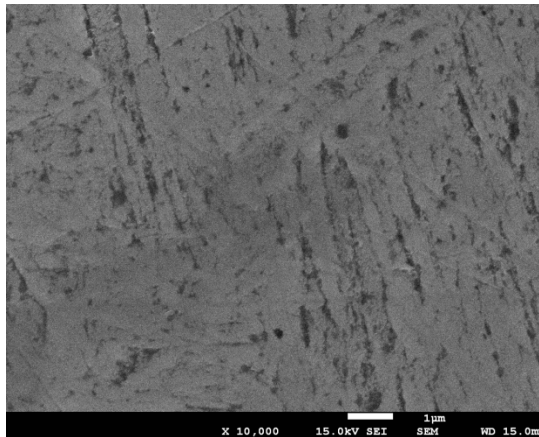


Fig. 3 SEM image of 1400 °C and 5 mm/s at 10,000× magnification on the surface

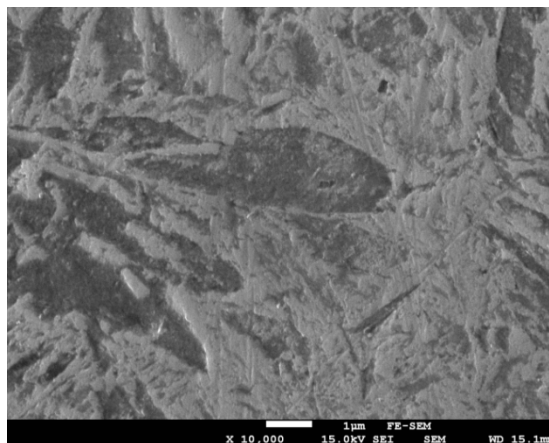


Fig. 4 SEM image of 1000 °C and 3 mm/s at 5000× magnification on the depth

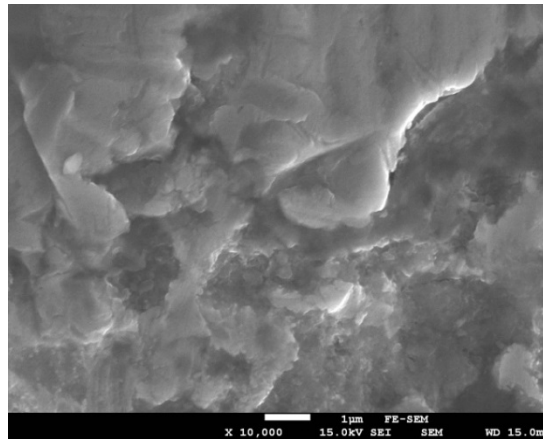


Fig. 5 SEM image of 1400 °C and 2 mm/s at 10000× magnification on the depth

3. The concept of fractals

When analysing the fractal dimensions, we used the R/S method. The R/S method (adjusted rescaled range method) or the adjusted scale is a graphical method and was selected for the estimation of the Hurst exponent. Hurst, the discoverer of the exponent that bears his name, studied power laws as they related to the Nile river floods. The adjusted scale of the partial summation area space component series deviates from the mean. Following Feder, the R/S analysis is as follows. Let the time series of natural phenomena in discrete time in the space component period τ be $\{x_1, x_2, \dots, x_n\}$. The calculation of the average distance m for the period t is presented in Eq. 1.

$$m = \frac{1}{n} \sum_{u=1}^n X_i \quad (1)$$

$Z(t)$ calculates as in Eq. 2.

$$Z(t) = \sum_{u=1}^t (X_i - m) \quad (2)$$

$R(n)$ calculates as in Eq. 3.

$$R(n) = \max(Z_1, Z_2, \dots, Z_n) - \min(Z_1, Z_2, \dots, Z_n) \quad (3)$$

$S(n)^2$ calculates as in Eq. 4.

$$S(n)^2 = \sum_{u=1}^t (X_i - m) \cdot (X_i - m) \quad (4)$$

Hurst observed the relationship R/S for a large number of natural phenomena and found the following empirical relationship in Eq. 5:

$$\frac{R}{S} = (c \tau)^H \quad (5)$$

The relationship between Hurst's exponent H and the Box-counting method for determining the fractal dimension D is very simple [10]. It is presented in Eq. 6 (in the plane) and Eq. 7 (in the space).

$$D = 2 - H \quad (6)$$

$$D = 3 - H \quad (7)$$

4. Results and discussions

We analysed the image format (e.g., JPEG) with 256 grey level numerical matrices (level 1 for black and 256 for white) with the program ImageJ. At each point (x, y) in the image (2D plane) the value of 1 to 256 is assigned. This value is then determined by a third coordinate in the 3D coordinate system, or z -coordinate. This means that the point $T = (x, y)$ plane is given by the third component and then forms $T3D = (x, y, z)$. This is presented in Figs. 6, 7, 8, and 9 which show the profile of a hardened specimen with certain parameters on the surface and in the depth. The graph of grey value presents the average of all lines on the y -axis. For each specimen, we have made an image of the microstructure at 5000 \times , 10,000 \times , 20,000 \times , 30,000 \times , and 50,000 \times magnification. Then, when we analysed the profile graphs and profiles, we found that the graphs are similar.

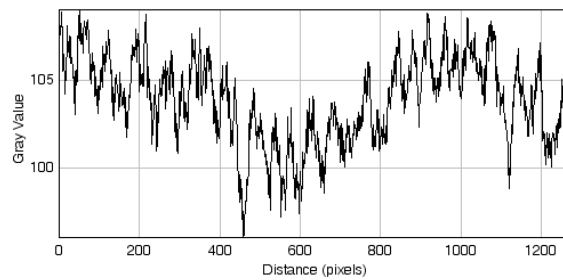


Fig. 6 Profile graph of surface pattern hardened by 2 mm/s at 1000 °C on surface

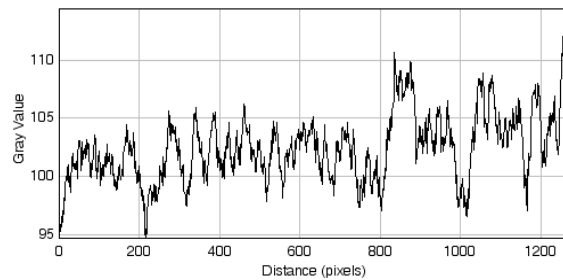


Fig. 7 Profile graph of depth pattern hardened by 3 mm/s at 1000 °C on depth

Comparing the profiles of the graphs we show the fractality of the robot laser-hardened specimens. The comparison is analysed with Hurst parameter H .

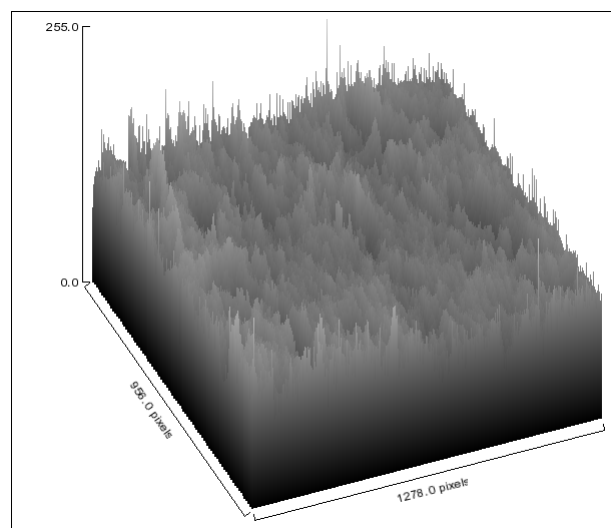


Fig. 8 Three-dimensional graph of the hardened surface of a sample of 2 mm/s at 1000 °C

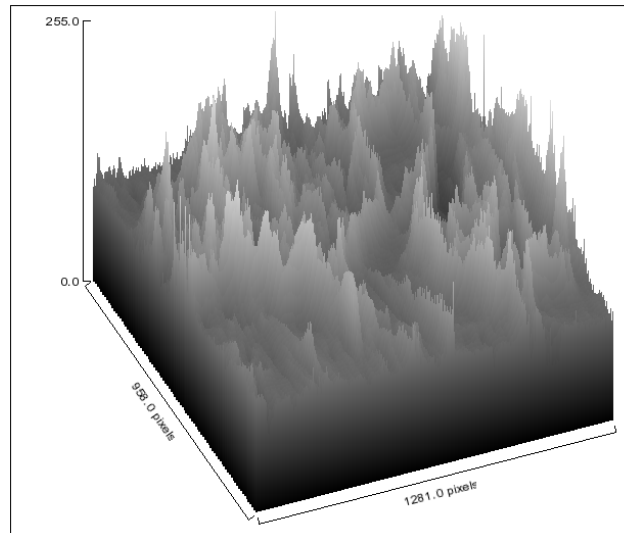


Fig. 9 Three-dimensional graph for of hardened surface of a sample at a depth of 3 mm/s at 1000 °C

For each specimen we calculated the fractal dimension at different magnifications. The results show that the fractal dimension is equal at different magnifications. With this we show the comparison of the microstructures of robot laser-hardened specimens.

Fig. 8 shows an example of the fractal structure of a robot laser-hardened specimen at 1000 °C with 2 mm/s velocity on the surface. Fig. 9 shows an example of the fractal structure of a robot laser-hardened specimen at 1000 °C with a 3 mm/s velocity at depth.

4.1 Influence of parameter temperature of robot laser cell on the fractal dimension

Fig. 10 and Fig. 11 show the relationship between temperature and speed of the robot laser hardening and fractal dimensions on the surface and at depth. If we increase the temperature of the robot laser cell, then the fractal dimension also increases. Fractal dimension is higher on the surface of robot laser hardening patterns. We can see that the fractal dimension decreased in a specimen when we increased the temperature.

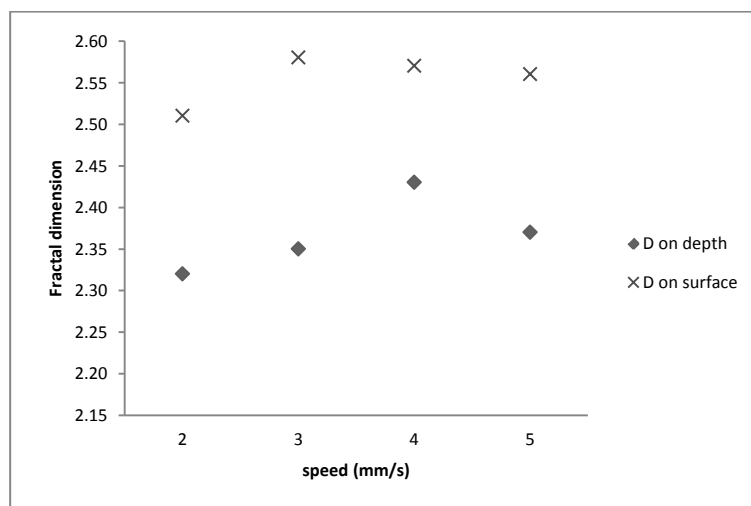


Fig. 10 Fractal dimension at 1000 °C at different speeds of hardening

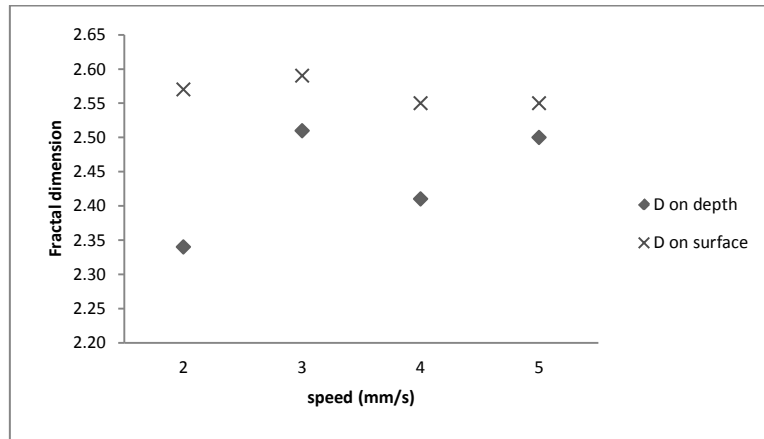


Fig. 11 Dimension at 1400 °C at different speeds of hardening

4.2 Influence of parameter velocity of robot laser cell on the fractal dimension

The speed of the robot laser cell impacts on hardening. We can see that the fractal dimension is higher in depth robot laser-hardened specimens. If we increase the velocity of the robot laser cell then that fractal dimension also increases. This also happens on the depth of robot laser-hardened specimens but differently.

4.3 Fractal dimension and hardness of specimen

Fig. 12 and Fig. 13 present the relationship between fractal dimension and the hardness of specimens hardened with different parameters of the robot laser cell. We can see that the specimen with the least fractal dimension is the hardest.

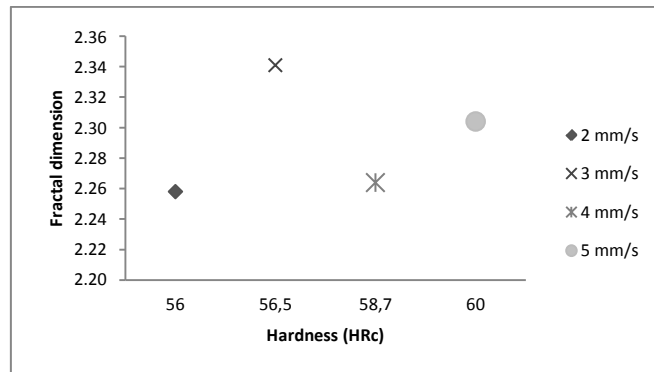


Fig. 12 The fractal dimension at 1000 °C at different speeds depending on hardness

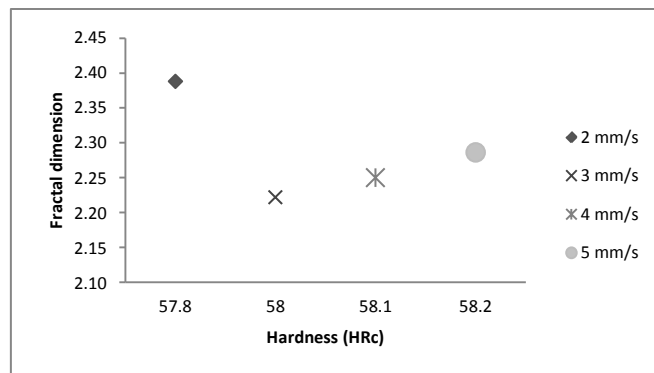


Fig. 13 The fractal dimension at 1400 °C at different speeds depending on hardness

For Fig. 12 and Fig. 13 we calculated the correlation coefficient, showing the size of the linear connection between hardness and fractal dimension. The correlation coefficient for Fig. 12 is $R = 0.0415$. The correlation coefficient for Fig. 13 is $R = 0.2446$. We can see that the correlation coefficients are not similar. Because the correlation coefficients are not 0, the variable hardness and fractal dimensions are correlated. The purpose of this work has been to study how the parameters of robot laser cells impact on the hardness of hardened specimens.

The fractal analysis of a series of digitized surface microstructures from the robot laser surface modified specimens indicated that useful correlations can be derived between the fractal dimensions and the surface microstructural features such as hardness.

5. Conclusion

Fractal structures are also found in robot laser-hardened samples when viewed under sufficient magnification. The hardening of various metal alloys has shown that when melting occurs, fractal geometry can be used to calculate the fractal dimension.

Using the R/S method, we analysed specimens of equal tempered metal after subjecting them to robot laser hardening using various parameters. The main findings can be summarized as follows:

- A fractal structure exists in robot laser hardening.
- The R/S method calculates the fractal dimensions for different parameters of laser hardening robotic cells.
- The optimal fractal dimensions of different parameter robotic laser-hardened tool steel have been identified.
- The fractal dimension varies between 2 and 3. By increasing the temperature of the robot laser cell, the fractal dimension becomes larger and the grain size becomes smaller. Consequently, we can use the fractal dimension as an important factor to define the grain shape.
- The dependence of the fractal dimension on hardness was ascertained. This finding is important if we know that certain alloys mix poorly because they have different melting temperatures, but such alloys have much higher hardness and better technical characteristics. By varying different parameters (temperature and speed), robot laser cells produce different fractal patterns with different fractal dimensions.
- Materials with higher fractal dimensions are less porous than those with lower fractal dimensions.
- Fractal dimension is higher in depth robot laser-hardened specimens.
- Specimens with lower fractal dimensions are the hardest.
- With the correlation coefficients we show a connection between the hardness and the fractal dimension of robot laser-hardened specimens.

The relationship between the microstructure and the parameters of robot laser cells may enable a better understanding of the fractal dimensions by exploring the microstructure.

In the future, we want to explore fractal dimension as a function of the parameters of a robot cell for laser hardening for pinned robot laser hardening: laser parameters such as power, energy density, focal distance, energy density in the focus, focal position, the shape of the laser flash, flash frequency, temperature and speed of hardening. We want to calculate fractal dimensions for different materials to ascertain the relationship between the materials and these parameters of the robot laser cell. We are interested in calculating the fractal dimensions in:

- Two-beam laser robot hardening (where the laser beam is divided into two parts).
- Areas of overlap (where the laser beam covers the already hardened area).
- Robot laser hardening at different angles (where the angles change depending on the x - and y -axes).

Acknowledgement

The present work was supported by the European Social Fund of the European Union.

References

- [1] Babič, M., Panjan, P., Kokol, P., Zorman, M., Belič, I., Verbovšek, T. (2013). Using fractal dimensions for determination of porosity of robot laser-hardened specimens, *International Journal of Computer Science Issues*, Vol. 10, No. 2, 184-190.
- [2] Mandelbrot, B.B. (1982). *The fractal geometry of nature*, W.H. Freeman and Company, New York.
- [3] Babič, M., Milfelner, M., Belič, I., Kokol, P. (2013). Problems associated with a robot laser cell used for hardening, *Materials and Technology*, Vol. 47, No. 1, 37-41.
- [4] Vollertsen, F., Partes, K., Meijer, J. (2005). State of the art of laser hardening and cladding, In: *Proceedings of the 3rd International WLT-Conference on Lasers in Manufacturing*, Munich, Germany, 281-305.
- [5] Pashby, I.R., Barnes, S., Bryden, B.G. (2003). Surface hardening of steel using a high power diode laser, *Journal of Materials Processing Technology*, Vol. 139, No. 1-3, 585-588, doi: [10.1016/S0924-0136\(03\)00509-0](https://doi.org/10.1016/S0924-0136(03)00509-0).
- [6] Tesar, J., Vacikova, P., Soukup, O., Houdkova, S. (2012). Infrared camera analysis of laser hardening, *Advances in Optical Technologies*, Vol. 2012, 1-6, doi: [10.1155/2012/593893](https://doi.org/10.1155/2012/593893).
- [7] El-Batahgy, A.-M., Ramadan, R.A., Moussa, A.-R. (2013). Laser surface hardening of tool steels – experimental and numerical analysis, *Journal of Surface Engineered Materials and Advanced Technology*, Vol. 3, No. 2, 146-153, doi: [10.4236/jsemat.2013.32019](https://doi.org/10.4236/jsemat.2013.32019).
- [8] Lima, M.S.F., Vasconcelos, G., Riva, R. (2012). Laser surface engineering as a tool for more efficient satellite components, *Journal of Aerospace Engineering, Sciences and Applications*, Vol. 4, No. 4, 105-111.
- [9] Feder, J. (1988). *Fractals*, Springer, New York.
- [10] Addison, P.S. (1997). *Fractals and chaos: an illustrated course*, Institute of Physics Publishing, London.
- [11] Xie, H.P., Liu, J.F., Ju, Y., Li, J., Xie, L.Z. (2011). Fractal property of spatial distribution of acoustic emissions during the failure process of bedded rock salt, *International Journal of Rock Mechanics and Mining Sciences*, Vol. 48, No. 8, 1344-1351, doi: [10.1016/j.ijrmms.2011.09.014](https://doi.org/10.1016/j.ijrmms.2011.09.014).
- [12] Li, J., Saharan, A., Koric, S., Ostoja-Starzewski, M. (2012). Elastic-plastic transition in three-dimensional random materials: massively parallel simulations, fractal morphogenesis and scaling functions, *Philosophical Magazine*, Vol. 92, No. 22, 2733-2758, doi: [10.1080/14786435.2012.674223](https://doi.org/10.1080/14786435.2012.674223).
- [13] Li, J., Ostoja-Starzewski, M. (2014). Fractal shear bands at elastic-plastic transitions in random Mohr-Coulomb materials, *Journal of Engineering Mechanics*, Vol. 140, No. 9, 04014072 (just released), doi: [10.1061/\(ASCE\)EM.1943-7889.0000750](https://doi.org/10.1061/(ASCE)EM.1943-7889.0000750).
- [14] Chaudhari, A., Sanders Yan, C.-C., Lee, S.-L. (2004). Multifractal analysis of growing surfaces, *Applied Surface Science*, Vol. 238, No. 1-4, 513-517, doi: [10.1016/j.apsusc.2004.05.247](https://doi.org/10.1016/j.apsusc.2004.05.247).
- [15] Yu, H.-S., Sun, X., Luo, S.-F., Wang, Y.-R., Wu, Z.-Q. (2002). Multifractal spectra of atomic force microscope images of amorphous electroless Ni-Cu-P alloy, *Applied Surface Science*, Vol. 191, No. 1-4, 123-127, doi: [10.1016/S0169-4332\(02\)00170-8](https://doi.org/10.1016/S0169-4332(02)00170-8).
- [16] Chen, Z.W., Lai, J.K.L., Shek, C.H. (2005). Multifractal spectra of scanning electron microscope images of SnO₂ thin films prepared by pulsed laser deposition, *Physics Letters A*, Vol. 345, No. 1-3, 218-223, doi: [10.1016/j.physleta.2005.05.104](https://doi.org/10.1016/j.physleta.2005.05.104).
- [17] Soković, M., Mikula, J., Dobrzański, L.A., Kopač, J., Koseč, L., Panjan, P., Madejski, J., Piech, A. (2005). Cutting properties of the Al₂O₃ + SiC_(w) based tool ceramic reinforced with the PVD and CVD wear resistant coatings, *Journal of Materials Processing Technology*, Vol. 164-165, 924-929, doi: [10.1016/j.jmatprotec.2005.02.071](https://doi.org/10.1016/j.jmatprotec.2005.02.071).